PSFC/JA-01-10

Equilibrium and Stability Properties of Self-Organized Electron Spiral Toroids

C. Chen, R. Pakter and D. C. Seward*

April 2001

Plasma Science and Fusion Center
Massachusetts Institute of Technology
Cambridge, MA 02139, USA

*Electron Power Systems, Inc.
42 Washington Drive
Acton, MA 01720, USA

This work was supported in part by Ballistic Missile Defense Organization, Contract No. DSWA01-97-M-0537. Reproduction, translation, publication, use and disposal, in whole or part, by or for the United States government is permitted.

Submitted for publication in *Physics of Plasmas.*

EQUILIBRIUM AND STABILITY PROPERTIES OF SELF-ORGANIZED ELECTRON SPIRAL TOROIDS

C. Chen and R. Pakter*
Plasma Science and Fusion Center
Massachusetts Institute of Technology
Cambridge, Massachusetts 02139

D. C. Seward
Electron Power Systems, Inc.
42 Washington Drive
Acton, Massachusetts 01720

ABSTRACT

A cold-fluid model for a self-organized electron spiral toroid (EST) is presented. In the present model, the electrons are assumed to undergo energetic spiral motion along a hollow torus with a fixed ion background, the electron mean free path is assumed to be long compared with the torus size, and the minor radius of the EST is assumed to be small compared with the major radius. Using this model, the equilibrium and stability properties of the electron flow in the self-organized EST are analyzed. It is found that a class of self-organized EST equilibria exists with or without an externally applied toroidal magnetic field. It is shown that in the absence of any applied toroidal magnetic field, the EST equilibria are stable at high electron densities (i.e., at high toroidal self-magnetic fields), although they are unstable at low electron densities (i.e., at low toroidal self-magnetic fields).

PACS: 41.75.F, 52.35, 52.55.H

*Permanent address: Departamento de Matematica, Universidade Luterana do Brasil, 92420-280, Canoas, RS, Brazil.

I. INTRODUCTION

Self-organized plasmas are often observed in nature. A well-known self-organized plasma is the so-called spheromak plasma [1] in which the magnetic field is produced almost entirely by the internal current flow in the plasma. Because no toroidal magnetic field is required outside the plasma (e.g., at the wall), spheromak plasmas can form spontaneuously given the appropriate initial conditions. Spheromak plasmas, which appear in the form of spheroids or toroids, have been studied theoretically [2-5] using magnetohydrodynamics (MHD) for more than five decades. Since the late 1950s, spheromak plasmas have been generated in various laboratories and have been studied experimentally [6-11], although there have been few detailed experimental studies of spontaneously generated spheromak plasmas in nature. The laboratory studies of spheromak plasmas were motivated by their potential applications in nuclear fusion [6-9], in terms of both a plasma confinement device [6,7] and a reactor fueling device [9], and in intense X-ray generation by accelerating and magnetically compressing the plasma [10,11].

Ball lightning [12] is another interesting self-organized plasma, but it is less understood. It is often observed during a lightning event in atmosphere. Both spherical and toroidal ball lightning plasmas have been reported [12]. Because the precise conditions for ball lightning to occur are still unknown, detailed properties of ball lightning plasmas, such as the energy density, have not been measured experimentally. Proposed theoretical models for ball lightning range from spheromak-like MHD models to dusty plasmas.

Recently, experimental evidence of self-organized toroidal plasmas in a DC arc discharge have been reported [13,14]. These self-organized plasma toroids, which are of 0.2 to 1 cm in diameter, appear to be stable for up to 0.6 seconds in partial atmosphere in the absense of any applied magnetic field. Because the electron mean free path is long compared with the diameter of the plasma under the partial atmosphere in these experiments, the electrons in such self-organized plasma have been postulated [13,14] to spiral energetically along a

torus with an ion background which is confined by the partial atmospheric pressure. These self-organized plasmas are referred to as self-organized electron spiral toroids [13]. Potential applications of self-organized electron spiral toroids include energy pulse formation, energy storage, and propulsion.

In this paper, we present a theoretical model for the self-organized electron spiral toroid (EST). In the present model, the electrons are assumed to undergo energetic spiral motion along a hollow torus with an ion background. The electron mean free path is assumed to be long compared with the EST size and the electron temperature is assumed to be low, so that the electrons are considered to form a hollow beam torus with cold-fluid motion. In the analysis, the electron temperature is assumed to be small. Because we are interested in the plasma dynamics on a time scale of the electron motion, the ion background is assumed to be fixed. Furthermore, the minor radius of the EST is assumed to be small compared with the major radius, i.e., the aspect ratio of the EST is assumed to be small. Consistent with the small aspect ratio assumption, the toroidal velocity of the electron flow is assumed to be negligibly small compared with the poloidal velocity of the electron flow. Using this model, the equilibrium and stability properties of the electron flow in the self-organized EST are analyzed. It is found that a class of self-organized EST equilibria exists without an externally applied toroidal magnetic field. It is shown that in the absence of any applied toroidal magnetic field, the EST equilibria are stable at high electron densities (i.e., at high toroidal self-magnetic fields), although they are unstable at low electron densities (i.e., at low toroidal self-magnetic fields).

The organization of this article is as follows. In Sec. II, a cold-fluid equilibrium theory of the electron spiral toroid (EST) is presented. Examples of tenuous and intense electron spiral toroids are presented. In Sec. III, use is made of the continuity equation, the force equation, and Maxwell's equations to obtain a complete set of linearized equations governing extraordinary mode perturbations. An eigenvalue equation for extraordinary mode purtur-

bations is derived, and solved numerically with a computer code. Detailed derivations of the extraordinary eigenmode equations including the boundary conditions are given in the Appendices at the end of this article. The results of the stability analyses of both tenuous and intense electron spiral toroids are discussed. In Sec. IV, the conclusions of this paper are presented.

II. EQUILIBRIUM THEORY

In this section, we present a cold-fluid equilibrium theory of the electron spiral toroid (EST). As stated in the Introduction, we make the following assumptions: a) the electron mean free path is assumed to be long compared with the EST size, so that the electrons are considered to form a hollow beam torus; b) the electron temperature is assumed to be low, so that a cold fluid description is used; c) the minor radius of the EST is assumed to be small compared with the major radius, so that the toroidal effects are negligibly small; and d) the ion background is assumed to be fixed. The last assumption implies that the equilibrium theory and subsequent stability analysis are valid in the time scale that is short in comparison with the time scale for the ion motion.

To the lowest order, we treat the toroidal flow in the EST with a small aspect ratio (i.e., with $r_{b2}/r_0 \ll 1$, where r_0 is the major EST radius) as if it flows along a straight cylinder, and analyze detailed equilibrium properties of the poloidal flow in the EST as shown in Fig. 1. In the poloidal coordinate system $(\rho, \phi, r_0\theta)$, the equilibrium electron density is assumed to be

$$n_b(\rho) = \begin{cases} \hat{n}_b r_{b1}/\rho, & r_{b1} < \rho < r_{b2}, \\ 0, & \text{otherwise.} \end{cases} \tag{1}$$

The equilibrium electron flow velocity has the general form

$$\vec{V}(\rho) = V_\phi(\rho)\vec{e}_\phi + V_\theta \vec{e}_\theta, \tag{2}$$

where $V_\theta \ll V_\phi$ and $V_\theta = \text{const}$. The fixed ion density is assumed to be

$$n_i(\rho) = f n_b(\rho), \tag{3}$$

where f is the ion fraction, which is slightly greater than unity.

It is readily shown that the equilibrium electron density and flow velocity, n_b and $\vec{V}$ defined in Eqs. (1) and (2), satisfy the steady-state continuity equation

$$-e\frac{\partial n_b}{\partial t} + \nabla \cdot \vec{J} = 0 \tag{4}$$

with $\partial/\partial t = 0$. In Eq. (4), $\vec{J} = -en_b\vec{V}$ is the electron current density and $-e$ is the electron charge.

The cold-fluid force balance equation for the equilibrium electron flow is

$$\frac{\partial \vec{V}}{\partial t} + (\vec{V}\cdot\nabla)\vec{V} = -\frac{e}{m}[\vec{E}^s + \vec{V}\times(B_0\vec{e}_\theta + \vec{B}^s)], \tag{5}$$

where $\partial/\partial t = 0$, m is the electron mass, $B_0\vec{e}_\theta$ is the applied toroidal magnetic field, and $\vec{E}^s = E^s_\rho(\rho)\vec{e}_\rho$ and $\vec{B}^s = B^s_\phi(\rho)\vec{e}_\phi + B^s_\theta(\rho)\vec{e}_\theta$ are the self-electric and self-magnetic fields produced by the electrons and background ions, respectively. Although an applied toroidal magnetic field is included in the present formation of the equilibrium and stability problem, it is set to be zero in all of the numerical examples presented later in this paper. The radial component of Eq. (5) is

$$\frac{V^2_\phi(\rho)}{\rho} = \frac{e}{m}\left\{E^s(\rho) + V_\phi(\rho)[B_0 + B^s_\theta(\rho)]\right\}, \tag{6}$$

where the negligibly small term $V_\theta B^s_\phi$ has been ignored. Solving Eq. (6) for $V_\phi(\rho)$ yields

$$V_\phi(\rho) = \frac{1}{2}\left\{\frac{e\rho}{m}(B_0 + B^s_\theta) \pm \left[\frac{e^2\rho^2}{m^2}(B_0 + B^s_\theta)^2 + \frac{4e\rho}{m}E^s_\rho\right]^{1/2}\right\}, \tag{7}$$

respectively.

The equilibrium Maxwell equations are:

$$\frac{1}{\rho}\frac{\partial}{\partial\rho}(\rho E^s_\rho) = -\frac{e(1-f)}{\epsilon_0}n_b(\rho), \tag{8}$$

$$\frac{\partial}{\partial\rho}B^s_\theta = \mu_0 e V_\phi(\rho)n_b(\rho). \tag{9}$$

Solving Eq. (8) for E^s_ρ with the boundary condition $E^s_\rho(\rho = 0) = 0$ yields

$$E^s_\rho(\rho) = \begin{cases} -(e/\epsilon_0)(1-f)\hat{n}_b r_{b1}(1 - r_{b1}/\rho), & r_{b1} < \rho < r_{b2}, \\ 0, & \rho < r_{b1}. \end{cases} \tag{10}$$

Substituting Eq. (7) into (9) yields

$$\frac{d}{d\rho}B^s_\theta = \frac{\mu_0 e}{2}n_b(\rho)\left\{\frac{e\rho}{m}(B_0 + B^s_\theta) \pm \left[\frac{e^2\rho^2}{m^2}(B_0 + B^s_\theta)^2 + \frac{4e\rho}{m}E^s_\rho\right]^{1/2}\right\}, \tag{11}$$

which has to be solved numerically under the boundary condition $B_\theta^s(\rho = r_{b2}) = 0$.

Use is made of a computer code, named CFTEST, to solve Eqs. (7) and (11) numerically. For present purposes, it is convenient to express Eqs. (7) and (11) in the following dimensionless forms (for $1 \leq \hat{\rho} \leq r_{b2}/r_{b1}$)

$$\hat{\omega}_b(\hat{\rho}) = \frac{1}{2}\left\{\hat{\Omega}^s + \hat{\Omega}_0 \pm \left[(\hat{\Omega}^s + \hat{\Omega}_0)^2 + 4(f-1)\frac{1}{\hat{\rho}}\left(1 - \frac{1}{\hat{\rho}}\right)\right]^{1/2}\right\}, \tag{12}$$

and

$$\frac{d\hat{\Omega}^s}{d\rho} = \frac{\alpha}{2}\left\{\hat{\Omega}^s + \hat{\Omega}_0 \pm \left[(\hat{\Omega}^s + \hat{\Omega}_0)^2 + 4(f-1)\frac{1}{\hat{\rho}}\left(1 - \frac{1}{\hat{\rho}}\right)\right]^{1/2}\right\}, \tag{13}$$

subject to the boundary condition

$$\hat{\Omega}^s\left(\frac{r_{b2}}{r_{b1}}\right) = 0. \tag{14}$$

In Eqs. (12) and (13), the dimensionless variables and parameters are defined by

$$\begin{aligned}
\hat{\rho} &= \frac{\rho}{r_{b1}}, \\
\hat{\omega}_b &= \frac{\omega_b}{\omega_p(r_{b1})} = \frac{V_\phi}{\rho\omega_p(r_{b1})}, \\
\hat{\Omega}^s &= \frac{\Omega^s}{\omega_p(r_{b1})} = \frac{eB_\theta^s}{m\omega_p(r_{b1})}, \\
\hat{\Omega}_0 &= \frac{\Omega_0}{\omega_p(r_{b1})} = \frac{eB_0}{m\omega_p(r_{b1})}, \\
\alpha &= \frac{r_{b1}^2\omega_p^2(r_{b1})}{c^2},
\end{aligned} \tag{15}$$

where

$$\omega_p(r_{b1}) = \left(\frac{e^2\hat{n}_b}{\epsilon_0 m}\right)^{1/2} \tag{16}$$

is the electron plasma frequency at $\rho = r_{b1}$, and c is the speed of light in *vacuo*.

Eqs. (12) and (13) are fully characterized by three dimensionless parameters, namely, α, a dimensionless measure of the electron density, f, the ratio of the background ion density to the electron density, and $\hat{\Omega}_0$, the normalized cyclotron frequency associated with the applied toroidal magnetic field. Moreover, since the variable $\hat{\rho}$ varies over the range from 1 to r_{b2}/r_{b1}

and the value of r_{b2}/r_{b1} can be chosen arbitrarily, we expect that EST equilibria exist over a wide range of system parameters.

Figure 2 shows a tenuous EST equilibrium as obtained numerically with the aid of the computer code in the absence of any applied toroidal magnetic field. The choice of system parameters in Fig. 2 corresponds to: $\alpha = 1.6$, $f = 1.02$, $\hat{\Omega}_0 = 0$, and $r_{b2}/r_{b1} = 1.01$. In this case, the EST equilibrium is tenuous because the Budker parameter is evaluated to be $\nu = (\alpha/2)(r_{b2}/r_{b1} - 1) = 8 \times 10^{-3}$, which is small compared with unity. In Fig. 2, the normalized cyclotron frequency $\Omega^s/\omega_p(r_{b1})$ and normalized electron angular flow velocity $\omega_b/\omega_p(r_{b1})$ are plotted as a function of the normalized minor radius ρ/r_{b1} for the clockwise-rotating electron flow in the tenuous EST equilibrium. For the clockwise-rotating electron flow, which corresponds to the minus sign in Eqs. (12) and (13), the electrons rotate in the positive $\vec{e}_\phi$-direction in reference to the schematic diagram shown in Fig. 1, and the self-magnetic field points out of the page because the current flow is in the negative $\vec{e}_\phi$-direction. In contrast, both the electron rotation and self-magnetic field for the counter-clockwise-rotating electron flow reverse their directions with respect to the clockwise-rotating electron flow.

With the choice of an inner minor radius of $r_{b1} = 4.95 \times 10^{-4}$ m and a major radius of $r_0 = 2.5 \times 10^{-3}$ m for the EST, we derive from Fig. 2 the following dimensional parameters: $r_{b2} = 5.00 \times 10^{-4}$ m, $V_\phi(r_{b2}) = 5.37 \times 10^6$ m/s, $B^s_\theta(r_{b1}) = -6.6 \times 10^{-4}$ Tesla, $N_b = 2.243 \times 10^{10}$, and $N_i = 2.288 \times 10^{10}$, where N_b is the total number of the electrons in the EST and N_i is the total number of the ions in the background.

Figure 3 shows plots of the normalized cyclotron frequency $\Omega^s/\omega_p(r_{b1})$ and normalized electron angular flow velocity $\omega_b/\omega_p(r_{b1})$ versus the normalized minor radius ρ/r_{b1} for the clockwise-rotating electron flow in an intense EST equilibrium as obtained numerically in the absence of any applied toroidal magnetic field for the choice of system parameters corresponding to: $\alpha = 1000$, $f = 1.0001$, $\hat{\Omega}_0 = 0$, and $r_{b2}/r_{b1} = 1.01$. In this case, the EST equilibrium

is intense because the Budker parameter is evaluated to be $\nu = (\alpha/2)(r_{b2}/r_{b1} - 1) = 5$, which is larger than unity. In comparison with the tenuous case shown in Fig. 2, we observe in Fig. 3 that the magnitude of the electron flow velocity increases rapidly at the outer edge of the EST. This trend becomes more pronounced as the Budker parameter increases. With the choice of an inner minor radius of $r_{b1} = 1.00 \times 10^{-2}$ m and a major radius of $r_0 = 0.1$ m for the EST, we derive from Fig. 3 the following dimensional parameters: $r_{b2} = 1.01 \times 10^{-2}$ m, $V_\phi(r_{b2}) = 9.49 \times 10^6$ m/s, $B^s_\theta(r_{b1}) = -1.49 \times 10^{-2}$ Tesla, $N_b = 5.609987 \times 10^{14}$, and $N_i = 5.610549 \times 10^{14}$, where N_b is the total number of the electrons in the EST and N_i is the total number of the ions in the background.

III. STABILITY ANALYSIS

In the present analysis, we consider extraordinary-mode perturbations on the cold-fluid EST equilibrium discussed in Sec. II. Under the extraordinary-mode perturbations, the electron density $n_b(\rho,\phi,t)$, electron flow velocity $\vec{V}(\rho,\phi,t)$, and electric and magnetic fields $\vec{E}(\rho,\phi,t)$ and $\vec{B}(\rho,\phi,t)$ in the EST can be expressed as

$$n_b(\rho,\phi,t) = n_b(\rho) + \delta n_b(\rho) e^{i(l\phi-\omega t)}, \tag{17}$$

$$\vec{V}(\rho,\phi,t) = V_\phi(\rho)\vec{e}_\phi + [\delta V_\rho(\rho)\vec{e}_\rho + \delta V_\phi(\rho)\vec{e}_\phi] e^{i(l\phi-\omega t)}, \tag{18}$$

$$\vec{E}(\rho,\phi,t) = E_\rho(\rho)\vec{e}_\rho + [\delta E_\rho(\rho)\vec{e}_\rho + \delta E_\phi(\rho)\vec{e}_\phi] e^{i(l\phi-\omega t)}, \tag{19}$$

$$\vec{B}(\rho,\phi,t) = B_\theta(\rho)\vec{e}_\theta + \delta B_\theta(\rho)\vec{e}_\theta e^{i(l\phi-\omega t)}. \tag{20}$$

In Eqs. (17)-(20), $l = \pm 1, \pm 2, \cdots$, ω is the frequency of the perturbations, ρ is the (minor) radial coordinate, ϕ is the poloidal angle, and θ is the toroidal angle; The quantities $n_b(\rho)$, $V_\phi(\rho)\vec{e}_\phi$, $E_\rho(\rho)\vec{e}_\rho$ and $B_\theta(\rho)\vec{e}_\theta$ are the electron density, flow velocity, and electric and magnetic fields in the cold-fluid EST equilibrium, respectively; The perturbations $\delta n_b(\rho,\phi,t) = \delta n_b(\rho) e^{i(l\phi-\omega t)}$, $\delta V_\phi(\rho,\phi,t) = [\delta V_\rho(\rho)\vec{e}_\rho + \delta V_\phi(\rho)\vec{e}_\phi] e^{i(l\phi-\omega t)}$, etc. are assumed to be small in the present analysis. Because an eigenmode with $\mathrm{Im}\omega > 0$ is *unstable*, we must show that all extraordinary modes have $\mathrm{Im}\omega \leq 0$ to prove that an EST equilibrium is stable against extraordinary-mode purturbations.

The aims of this section are to derive a complete set of linearized equations relating the perturbed quantities δn_b, δV_ρ, δV_ϕ, δE_ρ, δE_ϕ, and δB_θ, to derive the eigenvalue equation and appropriate boundary conditions, and to investigate the stability properties of both tenuous and intense ESTs. Consistent with the thin-beam approximation, the present analysis ignores curvature effects in the toroidal direction; that is, the unit vector $\vec{e}_\theta$ is considered as a constant unit vector. Detailed derivations are presented in Appendices A-D for an EST in open space (e.g., in air), and the results are summarized in Sec. III.A. The stability properties of tenuous and intense ESTs are discussed in Sec. III.B.

A. The Eigenvalue Problem

The stability problem of an EST can then be formulated as the following eigenvalue problem (for $r_{b1} < \rho < r_{b2}$)

$$\frac{1}{\rho}\frac{d}{d\rho}\left\{\frac{\rho}{1-\omega^2\rho^2/c^2l^2}[1+\chi_\rho(\omega,l,\rho)]\frac{d\delta\Phi}{d\rho}\right\} - \frac{l^2}{\rho^2}[1+\chi_\phi(\omega,l,\rho)]\delta\Phi = 0, \tag{21}$$

with the boundary conditions:

$$G^*(\rho = r_{b1}) = \frac{i}{2\pi r_{b1}c}\frac{J_l(\omega r_{b1}/c)}{J_l'(\omega r_{b1}/c)} \tag{22}$$

and

$$G^*(\rho = r_{b2}) = \frac{i}{2\pi r_{b2}c}\frac{H_l(\omega r_{b2}/c)}{H_l'(\omega r_{b2}/c)} \tag{23}$$

for an EST in open space (e.g., in air). In Eqs. (21)-(23), the eigenfunction $\delta\Phi$ is defined by

$$\delta\Phi = \delta\Phi(\rho) = \frac{i\rho}{l}\delta E_\phi(\rho). \tag{24}$$

The susceptibility functions $\chi_\rho(\omega,l,\rho)$ and $\chi_\phi(\omega,l,\rho)$ are defined by

$$\chi_\rho(\omega,l,\rho) = -\frac{\omega_p^2}{\nu_b^2}\frac{(1-\omega\omega_b\rho^2/c^2l)^2}{1-\omega^2\rho^2/c^2l^2}, \tag{25}$$

$$\begin{aligned}\chi_\phi(\omega,l,\rho) = &-\frac{\omega_p^2}{\nu_b^2}\left(1+\frac{\omega_p^2\rho^2/c^2l^2}{1-\omega^2\rho^2/c^2l^2}\right) + 2\frac{\omega_p^2}{\nu_b^2}\left(\frac{\Omega-2\omega_b}{l\omega}\right)\frac{\omega^2\rho^2/c^2l^2}{1-\omega^2\rho^2/c^2l^2} \\ &+\frac{1-\omega\omega_b\rho^2/c^2l}{(\omega-l\omega_b)(1-\omega^2\rho^2/c^2l^2)}\left(\frac{\rho}{l}\right)\frac{d}{d\rho}\left[\frac{\omega_p^2}{\nu_b^2}(\Omega-2\omega_b)\right],\end{aligned} \tag{26}$$

respectively, where $\Omega = \Omega^s + \Omega_0$. The function $\nu_b^2(\omega,l,\rho)$ is defined by

$$\nu_b^2(\omega,l,\rho) = (\omega-l\omega_b)^2\left[1+\frac{\omega_p^2\rho^2/c^2l^2}{1-\omega^2\rho^2/c^2l^2}\right] + (\Omega-2\omega_b)\left[\frac{1}{\rho}\frac{d}{d\rho}(\rho^2\omega_b) - \Omega\right]. \tag{27}$$

The admittance function $G(\rho)$ is defined by

$$G(\rho) \equiv \frac{\int_0^{2\pi}\delta E_\phi(\rho,\phi,t)\delta B_\theta^*(\rho,\phi,t)\rho d\phi}{|2\pi\rho\delta E_\phi(\rho,\phi,t)|^2} = \frac{1}{2\pi\rho}\frac{\delta B_\theta^*(\rho)}{\delta E_\phi^*(\rho)}, \tag{28}$$

which can be expressed explicitly as

$$G^*(\rho) = \left(\frac{i}{2\pi l}\right)\frac{1}{1-\omega^2\rho^2/c^2l^2}\times$$

$$\times \left\{ -\frac{\omega_p^2}{\nu_b^2}\left(\frac{1}{c^2 l}\right)(\Omega - 2\omega_b) + \left[\frac{\omega\rho}{c^2 l} - \frac{\omega_p^2}{\nu_b^2}\left(\frac{\rho}{c^2 l^2}\right)(\omega - l\omega_b)\frac{1 - \omega\omega_b\rho^2/c^2 l}{1 - \omega^2\rho^2/c^2 l^2}\right]\frac{1}{\delta\Phi}\frac{d\delta\Phi}{d\rho}\right\}. \quad (29)$$

The functions $J_l(x)$ and $H_l(x)$ are the first-kind Bessel and Hankel functions of order l, respectively.

Although the eigenvalue equation (21) resembles the extraordinary eigenvalue equation [15,16] describing the electron flow in crossed-field vacuum electron devices such as magnetrons and crossed-field amplifiers, there are significant differences. First, the present eigenvalue equation includes the effects of an fixed ion background which is absent in crossed-field vacuum electron devices. This allows us to analyze the stability properties of the self-organized EST in the absence of an applied toroidal magnetic field. Second, the present eivenvalue equation must be solved subject to the open boundary condition given in Eq. (23) rather than a closed conducting-wall boundary condition used in the analysis of crossed-field vacuum electron devices.

In the eigenvalue equation (21), there are two important resonances for the interaction between the electron flow and the perturbed wave fields, namely,

$$\omega - l\omega_b(\rho) \cong 0, \quad (30)$$

and

$$\nu_b^2(\omega, l, \rho) = (\omega - l\omega_b)^2\left[1 + \frac{\omega_p^2\rho^2/c^2 l^2}{1 - \omega^2\rho^2/c^2 l^2}\right] + (\Omega - 2\omega_b)\left[\frac{1}{\rho}\frac{d}{d\rho}(\rho^2\omega_b) - \Omega\right] \cong 0. \quad (31)$$

B. Numerical Results

A computer code, named CFTEST, has been developed for solving the eigenvalue problem defined in Eqs. (21)-(23). In the code, the standard shooting method is used to integrate the eigenvalue equation (21) from $\rho = r_{b1}$ to r_{b2}, and the boundary conditions in Eqs. (22) and (23). The code has been validated and is working correctly.

Use is made of CFTEST to investigate the stability properties of tenuous EST equilibria in the absence of any applied toroidal magnetic field. For the tenuous EST equilibrium

shown in Fig. 2 in Sec. II, the results of the stability analysis are summarized in Fig. 4. Figures 4(a) and 4(b) show, respectively, the normalized real eigenfrequency $\mathrm{Re}\omega/\omega_p(r_{b1})$ and normalized imaginary eigenfrequency $\mathrm{Im}\omega/\omega_p(r_{b1})$ as a function of the poloidal mode number l for the extraordinary eigenmode perturbations. As shown in Fig. 4, for each poloidal mode number l from $l = 1$ to 6 and for $l \geq 10$, there is a stable eigenmode with a real eigenfrequency. However, for each poloidal mode number l from $l = 7$ to 9, there is a pair of eigenmodes with complex eigenfrequencies. The eigenmodes with positive imaginary eigenfrequencies are unstable, whereas those with negative imaginary eigenfrequencies are damped. The maximum growth rate of the unstable eigenmodes is $\mathrm{Im}\omega_{max} \cong 0.005\ \omega_p(r_{b1})$, which occurs at $l = 8$. The real eigenfrequency increases as the poloidal mode number l increases, as expected from the resonance conditions in Eqs. (30) and (31).

As the electron density increases in the EST, i.e., as the parameter α increases, the growth rates of the instabilities shown in Fig. 4 decrease relative to the plasma frequency. This is illustrated in Fig. 5, in which the normalized imaginary eigenfrequency is plotted as a function of the parameter α for several unstable eigenmodes with the poloidal mode number $l = 5$, 6, 7 and 8. The choice of system parameters in Fig. 5 corresponds to: $\Omega_0 = 0$, $r_{b2}/r_{b1} = 1.01$, and $f - 1 = 0.032/\alpha$. In Fig. 5, the value of the parameter f is adjusted according to the relation $f - 1 = 0.032/\alpha$, so that the normalized electron poloidal flow velocity is fixed at $r_{b1}^2\omega_b^2(r_{b1})/c^2 = 3.2 \times 10^{-4}$ [see Eq. (7)]. It is evident in Fig. 5 that the normalized growth rate $\mathrm{Im}\omega/\omega_p(r_{b1})$ decreases as α increase. As a matter of fact, the relative maximum growth rate of the instabilities is found to slowly decrease to zero as the parameter α further increases, indicating stability for intense electron spiral toroids.

Use is also made of CFTEST to investigate the stability properties of intense EST equilibria in the absence of any applied toroidal magnetic field. All of the intense ESTs we investigated are found to be stable. As a typical example, the results of the stability analysis are summarized in Fig. 6 for the intense EST equilibrium shown in Fig. 3 in Sec. II. Figures

6(a) and 6(b) show, respectively, the normalized real frequency $\mathrm{Re}\omega/\omega_p(r_{b1})$ and normalized imaginary frequency $\mathrm{Im}\omega/\omega_p(r_{b1})$ as a function of the poloidal mode number l for the extraordinary eigenmode perturbations. The real frequency increases as the mode number l increases. The imaginary parts of the eigenfrequencies are either zero or negative. Therefore, all of the eigenmodes are stable. It is worthwhile noting that there are more eigenmodes in the intense case than in the tenuous case. The modes with higher frequencies correspond to higher-order radial oscillations.

IV. CONCLUSIONS

We have presented a cold-fluid model for a self-organized electron spiral toroid (EST) in partial atmosphere, assuming a) the electrons undergo energetic spiral motion along a hollow torus with an ion background, b) the electron mean free path is long compared with the EST size, c) the electron temperature is low, d) the ion background is assumed to be fixed, and e) the minor radius of the EST is small compared with the major radius. Using this model, the equilibrium and stability properties of the electron flow in the self-organized EST were analyzed.

In particular, the equilibrium poloidal electron flow velocity and equilibrium toroidal self-magnetic field were determined for a small-aspect ratio hollow EST. Examples of intense and tenuous EST equilibria were presented. Use was made of the continuity equation, the force equation, and Maxwell's equations to obtain a complete set of linearized equations governing extraordinary mode perturbations. An eigenvalue equation for extraordinary mode purturbations was derived, and solved numerically with a computer code. It was found that a class of self-organized EST equilibria exists without an externally applied toroidal magnetic field. It was shown that in the absence of any applied toroidal magnetic field, the EST equilibria are stable at high electron densities (i.e., at high toroidal self-magnetic fields), although they are unstable at low electron densities (i.e., at low toroidal self-magnetic fields).

APPENDIX A: LINEARIZED CONTINUITY, FORCE AND MAXWELL EQUATIONS

Under the extraordinary-mode perturbations given in Eqs. (17)-(20), the conservation of electron charge is maintained, which is described by the continuity equation

$$\frac{\partial}{\partial t} n_b(\rho,\phi,t) + \nabla \cdot [n_b(\rho,\phi,t)\vec{V}(\rho,\phi,t)] = 0. \tag{A1}$$

Linearizing Eq. (A1), we obtain

$$-i\omega\delta n_b + \frac{1}{\rho}\frac{d}{d\rho}(\rho n_b \delta V_\rho) + \frac{il}{\rho} n_b \delta V_\phi + \frac{il}{\rho} V_\phi \delta n_b = 0. \tag{A2}$$

From Eq. (A2), the density perturbation δn_b is given by

$$\delta n_b = \frac{1}{\omega - l\omega_b}\left[-\frac{i}{\rho}\frac{d}{d\rho}(\rho n_b \delta V_\rho) + \frac{l}{\rho} n_b \delta V_\phi \right], \tag{A3}$$

where the equilibrium electron angular flow velocity ω_b is defined by

$$\omega_b = \omega_b(\rho) = \frac{V_\phi(\rho)}{\rho}, \tag{A4}$$

which is a function of ρ.

The linearized force equation is given by

$$\frac{\partial}{\partial t}\delta\vec{V} + (V_\phi \vec{e}_\phi \cdot \nabla)\delta\vec{V} + (\delta\vec{V}\cdot\nabla)V_\phi\vec{e}_\phi = -\frac{e}{m}(\delta\vec{E} + V_\phi\vec{e}_\phi \times \delta\vec{B} + \delta\vec{V}\times B_\theta\vec{e}_\theta). \tag{A5}$$

Equation (A5) can be expressed in the component form

$$-i(\omega - l\omega_b)\delta V_\rho - 2\omega_b \delta V_\phi + \Omega\delta V_\phi = -\frac{e}{m}(\delta E_\rho + V_\phi \delta B_\theta), \tag{A6}$$

$$-i(\omega - l\omega_b)\delta V_\phi + \left[\frac{1}{\rho}\frac{d}{d\rho}(\rho^2\omega_b) - \Omega\right]\delta V_\rho = -\frac{e}{m}\delta E_\phi, \tag{A7}$$

where

$$\Omega = \Omega(\rho) = \frac{e}{m}[B_\theta^s(\rho) + B_0] \tag{A8}$$

is the electron cyclotron frequency in the equilibrium toroidal magnetic field $[B_\theta^s(\rho) + B_0]\vec{e}_\theta$.

The perturbed electric and magnetic fields $\delta\vec{E}(\rho,\phi,t)$ and $\delta\vec{B}(\rho,\phi,t)$ satisfy linearized Maxwell's equations

$$\nabla\cdot\delta\vec{E}(\rho,\phi,t) = -\frac{e}{\epsilon_0}\delta n_b(\rho,\phi,t), \tag{A9}$$

$$\nabla\times\delta\vec{E}(\rho,\phi,t) + \frac{\partial}{\partial t}\delta\vec{B}(\rho,\phi,t) = 0, \tag{A10}$$

$$\nabla\cdot\delta\vec{B}(\rho,\phi,t) = 0, \tag{A11}$$

$$\nabla\times\delta\vec{B}(\rho,\phi,t) - \frac{1}{c^2}\frac{\partial}{\partial t}\delta\vec{E}(\rho,\phi,t) = -\mu_0 e[n_b(\rho)\delta\vec{V}(\rho,\phi,t) + V_\phi(\rho)\vec{e}_\phi\delta n_b(\rho,\phi,t)]. \tag{A12}$$

Note that for $\delta\vec{B}(\rho,\phi,t) = \delta B_\theta(\rho)e^{i(l\phi-\omega t)}\vec{e}_\theta$, Eq. (A11) is automatically satisfied, i.e.,

$$\nabla\cdot\delta\vec{B}(\rho,\phi,t) = \frac{1}{\rho}\frac{\partial}{\partial(r_0\theta)}[\rho\delta B_\theta(\rho)e^{i(l\phi-\omega t)}] = 0, \tag{A13}$$

where r_0 is the major EST radius, and $r_0\theta$ is the displacement along the toroid. It should be reminded that the unit vector $\vec{e}_\theta$ is considered as a constant unit vector in the present analysis. Equations (A9), (A10) and (A12) can be expressed in the component form

$$\frac{1}{\rho}\frac{d}{d\rho}(\rho\delta E_\rho) + \frac{il}{\rho}\delta E_\phi = -\frac{e}{\epsilon_0}\delta n_b, \tag{A14}$$

$$\frac{1}{\rho}\frac{d}{d\rho}(\rho\delta E_\phi) - \frac{il}{\rho}\delta E_\rho = i\omega\delta B_\theta, \tag{A15}$$

$$\frac{il}{\rho}\delta B_\theta + \frac{i\omega}{c^2}\delta E_\rho = -\mu_0 e n_b\delta V_\rho, \tag{A16}$$

$$-\frac{d}{d\rho}\delta B_\theta + \frac{i\omega}{c^2}\delta E_\phi = -\mu_0 e(n_b\delta V_\phi + V_\phi\delta n_b). \tag{A17}$$

While there are four equations (A14)-(A17) for three field variables δE_ρ, δE_ϕ and δB_θ, we work with Eqs. (A15) and (A16) to obtain

$$\delta E_\rho = -\frac{1}{1-\omega^2\rho^2/c^2l^2}\left[\frac{d}{d\rho}\delta\Phi + \frac{i\omega\rho^2}{c^2l^2}\left(\frac{e}{\epsilon_0}\right)n_b\delta V_\rho\right] \tag{A18}$$

and

$$\delta B_\theta = \frac{1}{1-\omega^2\rho^2/c^2l^2}\left[\frac{\omega\rho}{c^2l}\frac{d}{d\rho}\delta\Phi + \frac{i\rho}{c^2l}\left(\frac{e}{\epsilon_0}\right)n_b\delta V_\rho\right], \tag{A19}$$

where $\delta\Phi(\rho)$ is defined in Eq. (24). Note that when $|\omega\rho/cl| \ll 1$, we have approximately

$$\delta E_\rho \cong -\frac{d}{d\rho}\delta\Phi, \quad \delta E_\phi \cong -\frac{il}{\rho}\delta\Phi, \quad \delta B_\theta \cong 0, \tag{A20}$$

corresponding to *electrostatic* perturbations.

To summarize briefly, equations (24), (A3), (A6), (A7), (A18) and (A19) relate the perturbed quantities δn_b, δV_ρ, δV_θ, δE_ρ, δE_ϕ, and δB_θ. These equations together with Poisson's equation (A14) will be used in Appendix B to derive an eigenvalue equation involving only $\delta\Phi(\rho) = (i\rho/l)\delta E_\phi(\rho)$.

APPENDIX B: DERIVATION OF THE EIGENVALUE EQUATION

The extraordinary-mode eigenvalue equation is derived in three major steps. As a first step, we eliminate the density perturbation δn_b in Eq. (A14) by substituting Eqs. (A3) and (A18) into Poisson's equation (A14). This readily gives

$$\frac{1}{\rho}\frac{d}{d\rho}\left(\frac{\rho}{1-\omega^2\rho^2/c^2l^2}\frac{d\delta\Phi}{d\rho}\right) - \frac{l^2}{\rho^2}\delta\Phi$$

$$= \frac{e}{\epsilon_0}\left\{-\frac{i}{\omega-l\omega_b}\frac{1}{\rho}\frac{d}{d\rho}(\rho n_b\delta V_\rho) - \frac{1}{\rho}\frac{d}{d\rho}\left[\frac{i\omega\rho^2/c^2l^2}{1-\omega^2\rho^2/c^2l^2}(\rho n_b\delta V_\rho)\right] + \frac{l/\rho}{\omega-l\omega_b}n_b\delta V_\phi\right\}. \quad (B1)$$

It is evident in Eq. (B1) that the field perturbation $\delta\Phi$ is driven self-consistently by the electron density perturbation which is now expressed in terms of the velocity perturbations δV_ρ and δV_ϕ.

As a second step, we express the velocity perturbations δV_ρ and δV_ϕ in terms of the field perturbation $\delta\Phi$ using the linearized force equations (A6) and (A7) and linearized Maxwell's equations (24), (A18) and (A19). Indeed, substituting Eqs. (A18) and (A19) into Eq. (A6), some straightforward algebra yields

$$(\omega-l\omega_b)\left[1+\frac{\omega_p^2\rho^2/c^2l^2}{1-\omega^2\rho^2/c^2l^2}\right]\delta V_\rho + i(\Omega-2\omega_b)\delta V_\phi = \frac{ie}{m}\,\frac{1-\omega V_\phi\rho/c^2l}{1-\omega^2\rho^2/c^2l^2}\,\frac{d\delta\Phi}{d\rho}, \quad (B2)$$

and substituting Eq. (24) into Eq. (A7) yields,

$$i\left[\frac{1}{\rho}\frac{d}{d\rho}(\rho^2\omega_b)-\Omega\right]\delta V_\rho + (\omega-l\omega_b)\delta V_\phi = -\frac{e}{m}\,\frac{l}{\rho}\delta\Phi. \quad (B3)$$

Solving Eqs. (B2) and (B3) for δV_ρ and δV_ϕ, we find that

$$\delta V_\rho = \frac{ie}{m\nu_b^2}\left[(\Omega-2\omega_b)\frac{l}{\rho}\delta\Phi + (\omega-l\omega_b)\frac{1-\omega V_\phi\rho/c^2l}{1-\omega^2\rho^2/c^2l^2}\,\frac{d\delta\Phi}{d\rho}\right], \quad (B4)$$

$$\delta V_\phi = \frac{e}{m\nu_b^2}\left\{\frac{1-\omega V_\phi\rho/c^2l}{1-\omega^2\rho^2/c^2l^2}\left[\frac{1}{\rho}\frac{d}{d\rho}(\rho^2\omega_b)-\Omega\right]\frac{d\delta\Phi}{d\rho} - (\omega-l\omega_b)\left[1+\frac{\omega_p^2\rho^2/c^2l^2}{1-\omega^2\rho^2/c^2l^2}\right]\frac{l}{\rho}\delta\Phi\right\}, \quad (B5)$$

where the quantity $\nu_b^2 = \nu_b^2(\omega, l, \rho)$ is defined in Eq. (27).

As a third step, we substitute Eqs. (B4) and (B5) into Eq. (B1) to obtain the eigenvalue equation

$$\begin{aligned}
&\frac{1}{\rho}\frac{d}{d\rho}\left(\frac{\rho}{1-\omega^2\rho^2/c^2l^2}\frac{d\delta\Phi}{d\rho}\right) - \frac{l^2}{\rho^2}\left[1-\frac{\omega_p^2}{\nu_b^2}\left(1+\frac{\omega_p^2\rho^2/c^2l^2}{1-\omega^2\rho^2/c^2l^2}\right)\right]\delta\Phi \\
&= \frac{1}{\omega-l\omega_b}\frac{1}{\rho}\frac{d}{d\rho}\left\{\rho\frac{\omega_p^2}{\nu_b^2}\left[(\Omega-2\omega_b)\frac{l}{\rho}\delta\Phi+(\omega-l\omega_b)\frac{1-\omega V_\phi\rho/c^2l}{1-\omega^2\rho^2/c^2l^2}\frac{d\delta\Phi}{d\rho}\right]\right\} \qquad (B6)\\
&+\frac{1}{\rho}\frac{d}{d\rho}\left\{\rho\frac{\omega_p^2}{\nu_b^2}\frac{\omega\rho^2/c^2l^2}{1-\omega^2\rho^2/c^2l^2}\left[(\Omega-2\omega_b)\frac{l}{\rho}\delta\Phi+(\omega-l\omega_b)\frac{1-\omega V_\phi\rho/c^2l}{1-\omega^2\rho^2/c^2l^2}\frac{d\delta\Phi}{d\rho}\right]\right\} \\
&+\frac{l\omega_p^2}{\rho\nu_b^2}\frac{1}{\omega-l\omega_b}\frac{1-\omega V_\phi\rho/c^2l}{1-\omega^2\rho^2/c^2l^2}\left[\frac{1}{\rho}\frac{d}{d\rho}(\rho^2\omega_b)-\Omega\right]\frac{d\delta\Phi}{d\rho},
\end{aligned}$$

where $l=\pm1,\pm2,\cdots$, and $\omega_p(\rho)=[e^2n_b(\rho)/\epsilon_0 m]^{1/2}$ is the (local) electron plasma frequency.

Finally, after a lengthy algebraic exercise, we can express the eigenvalue equation (B6) in the following form

$$\frac{1}{\rho}\frac{d}{d\rho}\left\{\frac{\rho}{1-\omega^2\rho^2/c^2l^2}[1+\chi_\rho(\omega,l,\rho)]\frac{d\delta\Phi}{d\rho}\right\} - \frac{l^2}{\rho^2}[1+\chi_\phi(\omega,l,\rho)]\delta\Phi=0, \qquad (B7)$$

where the susceptibility functions $\chi_\rho(\omega,l,\rho)$ and $\chi_\phi(\omega,l,\rho)$ are defined in Eqs. (25) and (26), respectively.

Equation (B7) must be solved subject to appropriate boundary conditions. For an EST in open space (e.g., in air), the boundary conditions are

$$\delta\Phi(\rho=0)=0 \quad \text{and} \quad \delta\Phi(\rho=\infty)\propto\rho^{1/2}. \qquad (B8)$$

Consistent with the boundary conditions in Eq. (B8), the boundary conditions at $\rho=r_{b1}$ and r_{b2} will be derived in Appendix D after a brief discussion of the solutions to Eq. (B7) in the vacuum regions in Appendix C.

APPENDIX C: SOLUTIONS IN THE VACUUM REGIONS

We solve the eigenvalue equation (B7) in the vacuum regions with $\rho < r_{b1}$ and with $\rho > r_{b2}$, where $n_b(\rho) = \delta n_b(\rho) = \delta V_\phi(\rho) = \delta V_\rho(\rho) = 0$. For $\rho < r_{b1}$ or $\rho > r_{b2}$, Eq. (B7) can expressed as

$$\frac{1}{\rho}\frac{d}{d\rho}\left(\frac{\rho}{1-\omega^2\rho^2/c^2l^2}\frac{d\delta\Phi}{d\rho}\right) - \frac{l^2}{\rho^2}\delta\Phi = 0 \tag{C1}$$

or

$$\frac{d^2\delta\Phi}{d\rho^2} + \frac{1}{\rho}\frac{1+\omega^2\rho^2/c^2l^2}{1-\omega^2\rho^2/c^2l^2}\frac{d\delta\Phi}{d\rho} + \left(\frac{\omega^2}{c^2} - \frac{l^2}{\rho^2}\right)\delta\Phi = 0. \tag{C2}$$

While neither Eq. (C1) nor Eq. (C2) seems to be analytically tractable, we can solve for $\delta\Phi$ *indirectly* by returning to Eqs. (A14)-(A17). Setting $n_b(\rho) = \delta n_b(\rho) = \delta V_\phi(\rho) = \delta V_\rho(\rho) = 0$, we express Eqs. (A14)-(A17) as

$$\frac{1}{\rho}\frac{d}{d\rho}(\rho\delta E_\rho) + \frac{il}{\rho}\delta E_\phi = 0, \tag{C3}$$

$$\frac{1}{\rho}\frac{d}{d\rho}(\rho\delta E_\phi) - \frac{il}{\rho}\delta E_\rho = i\omega\delta B_\theta, \tag{C4}$$

$$\frac{il}{\rho}\delta B_\theta + \frac{i\omega}{c^2}\delta E_\rho = 0, \tag{C5}$$

$$-\frac{d}{d\rho}\delta B_\theta + \frac{i\omega}{c^2}\delta E_\phi = 0. \tag{C6}$$

We have from Eq. (C3),

$$\delta E_\phi = -\frac{1}{il}\frac{d}{d\rho}(\rho\delta E_\rho), \tag{C7}$$

and from Eq. (C5),

$$\delta B_\theta = -\frac{\omega\rho}{lc^2}\delta E_\rho. \tag{C8}$$

Substituting Eqs. (C7) and (C8) into Eq. (C4) yields Bessel's equation

$$\frac{1}{\rho}\frac{d}{d\rho}\left[\rho\frac{d}{d\rho}(\rho\delta E_\rho)\right] + \left(\frac{\omega^2}{c^2} - \frac{l^2}{\rho^2}\right)(\rho\delta E_\rho) = 0 \tag{C9}$$

for the variable $\rho\delta E_\rho$.

General solutions to Eq. (C9) are

$$\rho\delta E_\rho(\rho) = CJ_l(\omega\rho/c) + DY_l(\omega\rho/c), \tag{C10}$$

where $J_l(x)$ and $Y_l(x)$ are the first- and second-kind Bessel functions of order l, and C and D are constants to be determined by the boundary conditions given in Eq. (B8) together with solutions to Eq. (B7) within the EST electron layer ($r_{b1} < \rho < r_{b2}$). Substituting Eqs. (C7) and (C10) into Eq. (24), we obtain general solutions to the eigenvalue equation in the vacuum regions outside the EST electron layer with $\rho < r_{b1}$ and with $\rho > r_{b2}$,

$$\delta\Phi(\rho) = -\frac{\omega\rho}{l^2 c}[CJ_l'(\omega\rho/c) + DY_l'(\omega\rho/c)], \tag{C11}$$

where $J_l'(x) = dJ_l(x)/dx$ and $Y_l'(x) = dY_l(x)/dx$.

We now find special solutions for an EST in open space by taking into account the boundary conditions given in Eq. (B8). In the inner vacuum region with $0 \leq \rho < r_{b1}$, $D = 0$, because all of the field perturbations must be finite at $\rho = 0$. Therefore, for $0 \leq \rho < r_{b1}$, the eigenfunction $\delta\Phi(\rho)$ can be expressed as

$$\delta\Phi(\rho) = -\frac{\omega\rho}{l^2 c}C_< J_l'(\omega\rho/c), \tag{C12}$$

and the corresponding perturbed fields are given by

$$\begin{aligned} \delta B_\theta(\rho) &= -\frac{\omega}{lc^2}C_< J_l(\omega\rho/c), \\ \delta E_\rho(\rho) &= \frac{C_<}{\rho}J_l(\omega\rho/c), \\ \delta E_\phi(\rho) &= \frac{i\omega}{lc}C_< J_l'(\omega\rho/c). \end{aligned} \tag{C13}$$

Here, $C_<$ is a constant to be determined by the boundary conditions at $\rho = r_{b1}$.

In the outer vacuum region with $\rho > r_{b2}$, $D = iC$, because the perturbed fields form an out-going wave. Therefore, for $\rho > r_{b2}$, the eigenfunction $\delta\Phi(\rho)$ can be expressed as

$$\delta\Phi(\rho) = -\frac{\omega\rho}{l^2 c}C_> H_l'(\omega\rho/c), \tag{C14}$$

where $H_l(x)$ is the first-kind Hankel function of order l defined by

$$H_l(x) = J_l(x) + iY_l(x). \tag{C15}$$

The corresponding perturbed fields are given by

$$\delta B_\theta(\rho) = -\frac{\omega}{lc^2} C_> H_l(\omega\rho/c),$$
$$\delta E_\rho(\rho) = \frac{C_>}{\rho} H_l(\omega\rho/c), \qquad (C16)$$
$$\delta E_\phi(\rho) = \frac{i\omega}{lc} C_> H_l'(\omega\rho/c).$$

Here, $C_>$ is a constant to be determined by the boundary conditions at $\rho = r_{b2}$.

The rms radial Poynting flux is

$$P(\rho) = \frac{1}{2}\delta E_\phi(\rho)\delta B_\theta^*(\rho)\exp(2\mathrm{Im}\omega t) = -\frac{i}{2}\frac{|\omega|^2}{l^2c^3}|C_>|^2 H_l'(\omega\rho/c)H_l^*(\omega\rho/c)\exp(2\mathrm{Im}\omega t), \qquad (C17)$$

for $\rho > r_{b2}$. If the EST is stable with $\mathrm{Im}\omega \leq 0$, then the Poynting flux is small under small purturbations. On the other hand, if the EST is unstable with $\mathrm{Im}\omega > 0$, then the Poynting flux increases exponentially as a function of time as purturbations grow, reducing the lifetime of the EST.

APPENDIX D: DERIVATION OF BOUNDARY CONDITIONS

To solve the eigenvalue equation (B7) numerically in the electron layer from $\rho = r_{b1}$ to r_{b2}, we must set the boundary conditions at the inner and outer surfaces of an EST. For present purposes, we introduce the admittance defined in Eq. (29), which is the ratio between the radial Poynting flow per unit length in the θ-direction and the square of the (effective) voltage associated with δE_ϕ. Since both $\delta E_\phi(\rho)$ and the radial Poynting flux are continuous, it follows that the admittance G is *continuous* at $\rho = r_{b1}$ and $\rho = r_{b2}$.

For an EST in open space (e.g., in air), the boundary conditions can be derived with the aid of the special solutions obtained in Appendix C and the continuity of the admittance at the EST surfaces. Substituting Eq. (C13) into Eq. (28), and setting $\rho = r_{b1} - 0$, we obtain

$$G^*(\rho = r_{b1} - 0) = \frac{i}{2\pi r_{b1} c} \frac{J_l(\omega r_{b1}/c)}{J_l'(\omega r_{b1}/c)}. \tag{D1}$$

Similarly, substituting Eq. (C16) into Eq. (28), and setting $\rho = r_{b2} + 0$, we obtain

$$G^*(\rho = r_{b2} + 0) = \frac{i}{2\pi r_{b2} c} \frac{H_l(\omega r_{b2}/c)}{H_l'(\omega r_{b2}/c)}. \tag{D2}$$

Evidently, one of the advantages of introducing the admittance G is that the coefficients $C_<$ and $C_>$ do not appear explicitly in Eqs. (D1) and (D2).

Inside the EST electron layer, an analytical expression for the admittance G can be obtained by substituting Eqs. (24), (A20) and (B4) into Eq. (28). This gives (for $r_{b1} \le \rho \le r_{b2}$)

$$G^*(\rho) = \left(\frac{i}{2\pi l}\right) \frac{1}{1 - \omega^2\rho^2/c^2l^2} \times$$
$$\times \left\{ -\frac{\omega_p^2}{\nu_b^2} \left(\frac{1}{c^2 l}\right) (\Omega - 2\omega_b) + \left[\frac{\omega\rho}{c^2 l} - \frac{\omega_p^2}{\nu_b^2} \left(\frac{\rho}{c^2 l^2}\right) (\omega - l\omega_b) \frac{1 - \omega\omega_b\rho^2/c^2 l}{1 - \omega^2\rho^2/c^2 l^2}\right] \frac{1}{\delta\Phi} \frac{d\delta\Phi}{d\rho} \right\}. \tag{D3}$$

Since $G^*(\rho)$ is continuous at $\rho = r_{b1}$ and r_{b2}, we obtain the following boundary conditions

$$G^*(\rho = r_{b1}) = \frac{i}{2\pi r_{b1} c} \frac{J_l(\omega r_{b1}/c)}{J_l'(\omega r_{b1}/c)}, \tag{D4}$$

and

$$G^*(\rho = r_{b2}) = \frac{i}{2\pi r_{b2} c} \frac{H_l(\omega r_{b2}/c)}{H_l'(\omega r_{b2}/c)}, \tag{D5}$$

where $G^*(\rho)$ is defined in Eq. (29) for $r_{b1} < \rho < r_{b2}$. This concludes the derivation of the boundary conditions in Eqs. (22) and (23).

ACKNOWLEDGMENT

This work was supported in part by Ballistic Missile Defense Organization, Contract No. DSWA01-97-M-0537. The Authors wish to thank Dr. William Guss for providing helpful comments about this paper.

REFERENCES

1. P. M. Bellan, *Spheromaks: A Practical Application of Magnetohydrodynamic Dynamos and Plasma Self-Organization* (Imperial College Press, NJ 2000) and references therein.

2. S. Lundquist, Arkiv for Fysik **B2**, 361 (1950).

3. H. P. Furth, M. A. Levine, and R. W. Waniek, Rev. Sci. Instrum. **28**, 949 (1957).

4. L. W. Woltjer, Proc. Nat. Acad. Sci. (USA) **44**, 490 (1958); Proc. Nat. Acad. Sci. (USA) **44**, 833 (1958)

5. J. B. Taylor, Phys. Rev. Lett. **33**, 1139 (1974).

6. W. H. Bostick, Sci. Amer. **197**, 87 (1957).

7. H. Alfvén, L. Lindberg, and P. Mitlid, J. Nucl. Energy (Part C) **1**, 116 (1959).

8. D. R. Wells, Phys. Fluids **7**, 826 (1964).

9. R. Raman, et al., Phys. Rev. Lett. **73**, 3101 (1993).

10. J. H. Hammer, C. W. Hartman, J. L. Eddleman, and H. S. McLean, Phys. Rev. Lett. **61**, 2843 (1988).

11. J. H. Degnan, et al., Phys. Fluids **B5**, 2938 (1993).

12. See, for example, M. A. Uman, *The Lightning Discharge* (Academic Press, New York, 1987).

13. D. C. Seward, C. Chen, R. Pakter, "Electron Spiral Toroids," Bulletin American Physical Society **43**, 1695 (1998).

14. D. C. Seward, D. C. Seward, W. C. Guss, and C. Chen, "Self-Organized Micro-Toroids Generated in a Vacuum-Arc," Bulletin American Physical Society **45**, 303 (2000).

15. R. C. Davidson and K. T. Tsang, Phys. Fluids 29, 3832 (1986).

16. R. C. Davidson, H. W. Chan, C. Chen, and S. Lund, Rev. Mod. Phy. **63**, 341 (1991).

FIGURE CAPTIONS

Fig. 1 Cross section of an electron spiral toroid showing the poloidal electron flow $V_\phi(\rho)\vec{e}_\phi$ and poloidal coordinate system (ρ, ϕ, θ) with $\vec{e}_\theta$ pointing into the page.

Fig. 2 Plots of (a) normalized cyclotron frequency $\Omega^s/\omega_p(r_{b1})$ and (b) normalized electron angular flow velocity $\omega_b/\omega_p(r_{b1})$ versus the normalized minor radius ρ/r_{b1} for the clockwise-rotating electron flow in a tenuous EST equilibrium. The choice of system parameters corresponds to: $\alpha = 1.6$, $f = 1.02$, $\Omega_0 = 0$, and $r_{b2}/r_{b1} = 1.01$.

Fig. 3 Plots of (a) normalized cyclotron frequency $\Omega^s/\omega_p(r_{b1})$ and (b) normalized electron angular flow velocity $\omega_b/\omega_p(r_{b1})$ versus the normalized minor radiusρ/r_{b1} for the clockwise-rotating electron flow in an intense EST equilibrium. The choice of system parameters corresponds to: $\alpha = 1000$, $f = 1.0001$, $\Omega_0 = 0$, and $r_{b2}/r_{b1} = 1.01$.

Fig. 4 Plots of (a) normalized real eigenfrequency $\mathrm{Re}\omega/\omega_p(r_{b1})$ and (b) normalized imaginary eigenfrequency $\mathrm{Im}\omega/\omega_p(r_{b1})$ versus the poloidal mode number l for a tenuous EST with the same choice of system parameters as shown in Fig. 2.

Fig. 5 Plot of the normalized imaginary eigenfrequency $\mathrm{Im}\omega/\omega_p(r_{b1})$ versus the dimensionless parameter $\alpha = r_{b1}^2\omega_p^2(r_{b1})/c^2$ for several values of the poloidal mode mumber l. Here, the choice of system parameters corresponds to: $\Omega_0 = 0$, $r_{b2}/r_{b1} = 1.01$, and $f - 1 = 0.032/\alpha$.

Fig. 6 Plots of (a) normalized real eigenfrequency $\mathrm{Re}\omega/\omega_p(r_{b1})$ and (b) normalized imaginary eigenfrequency $\mathrm{Im}\omega/\omega_p(r_{b1})$ versus the poloidal mode number l for an intense EST with the same choice of system parameters as shown in Fig. 3.

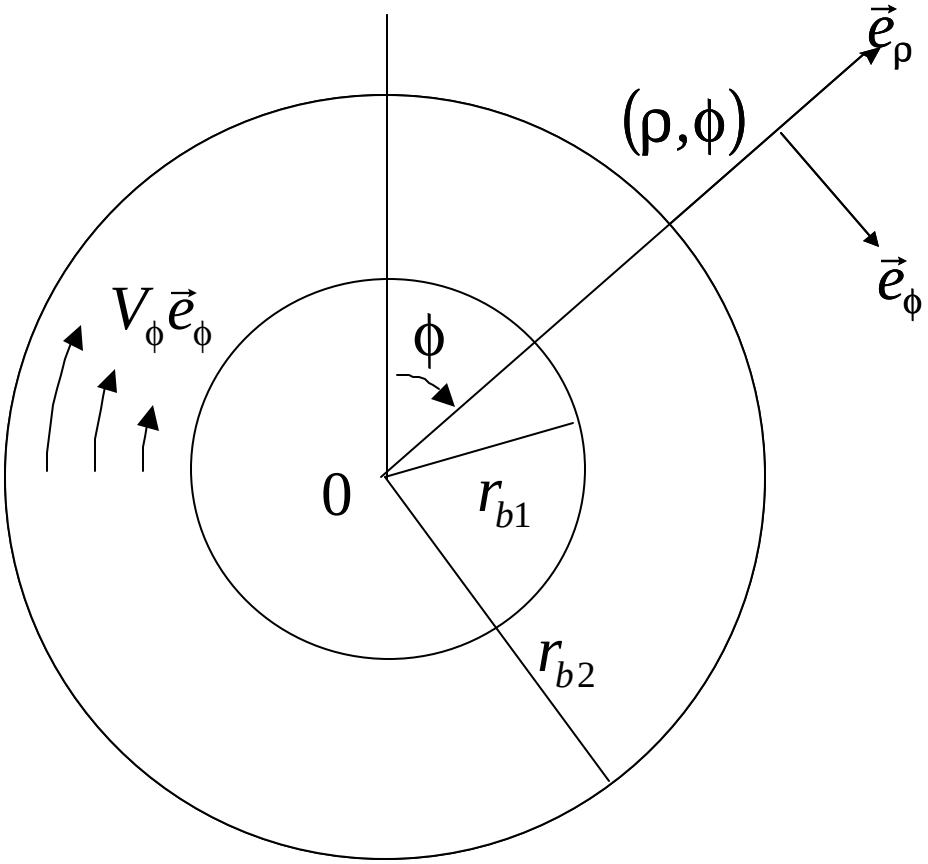

Fig. 1

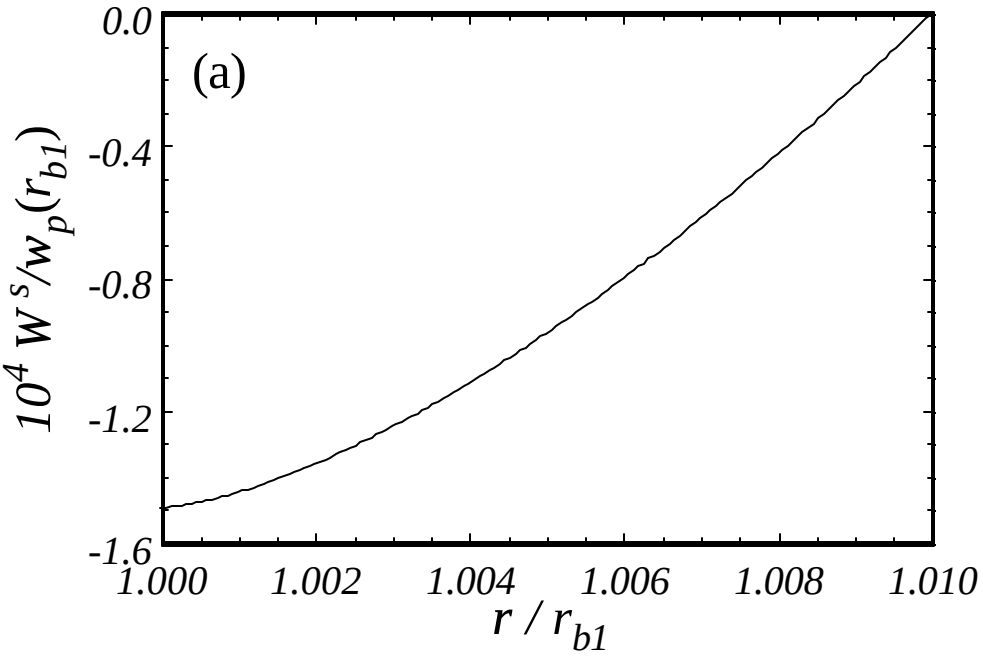
(a)
0.0
-0.4
-0.8
-1.2
-1.6
1.000
1.002
1.004
1.006
1.008
1.010
$10^4\, w^s/w_p(r_{b1})$
r / r_{b1}

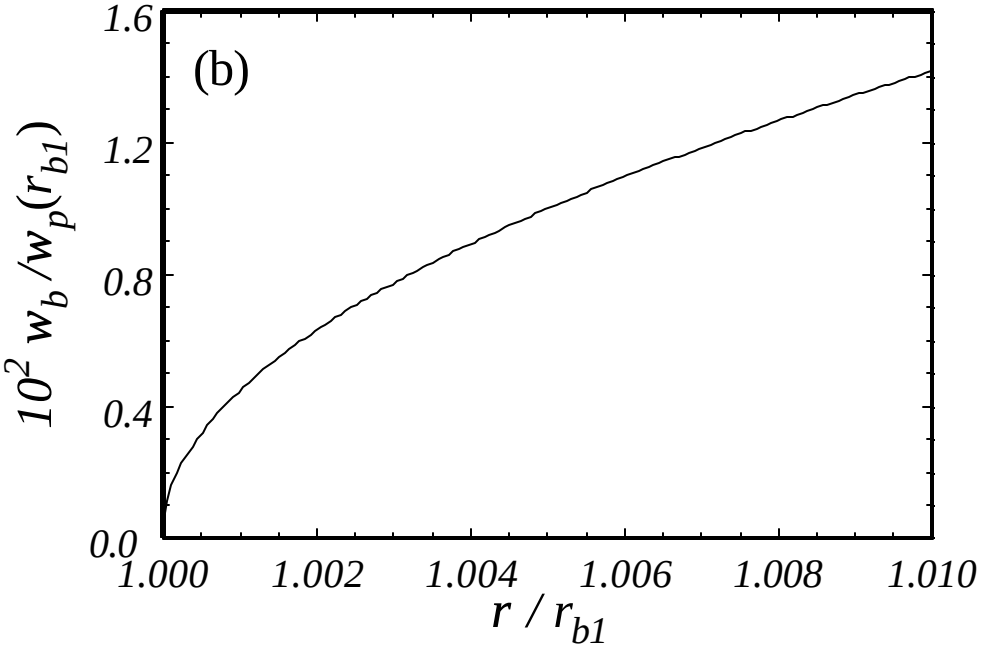
(b)
1.6
1.2
0.8
0.4
0.0
1.000
1.002
1.004
1.006
1.008
1.010
$10^2\, w_b/w_p(r_{b1})$
r / r_{b1}

Fig. 2

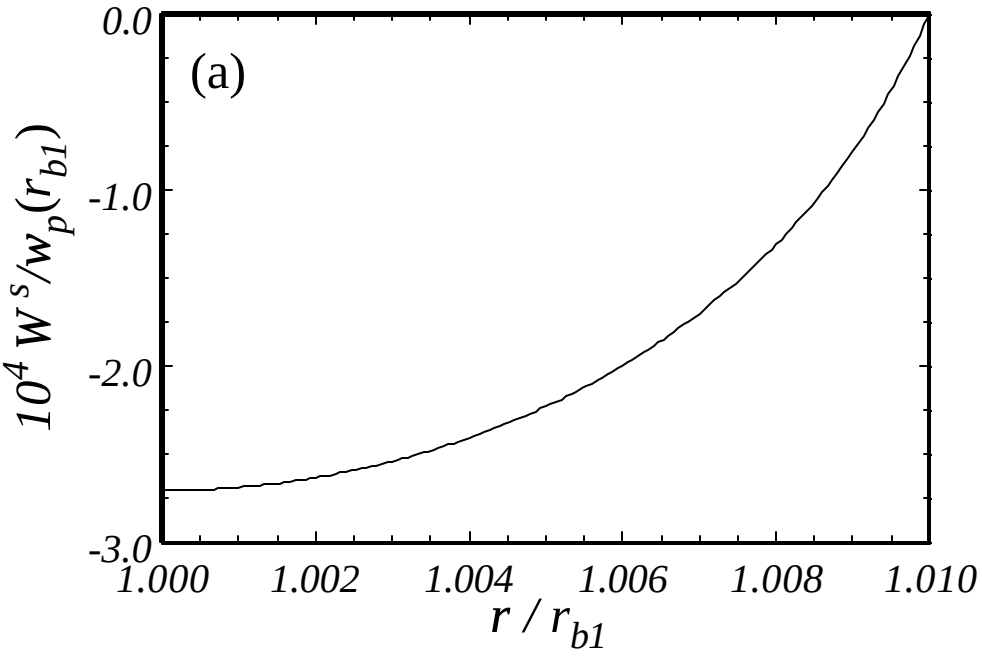
(a)
0.0
-1.0
-2.0
-3.0
$10^4\, w^s / w_p(r_{b1})$
1.000
1.002
1.004
1.006
1.008
1.010
r / r_{b1}

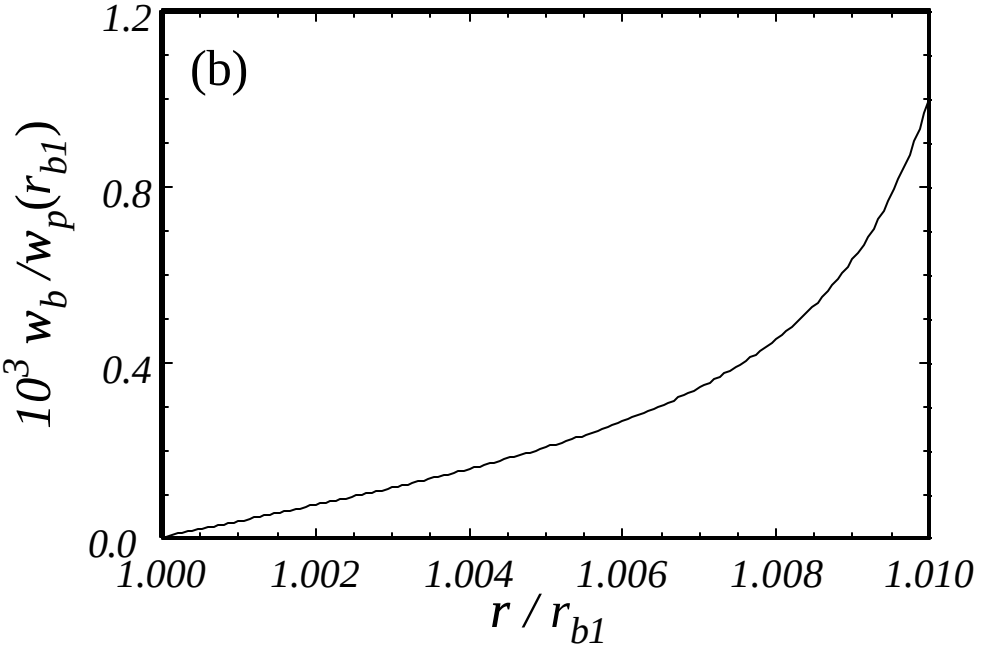
(b)
1.2
0.8
0.4
0.0
$10^3\, w_b / w_p(r_{b1})$
1.000
1.002
1.004
1.006
1.008
1.010
r / r_{b1}

Fig. 3

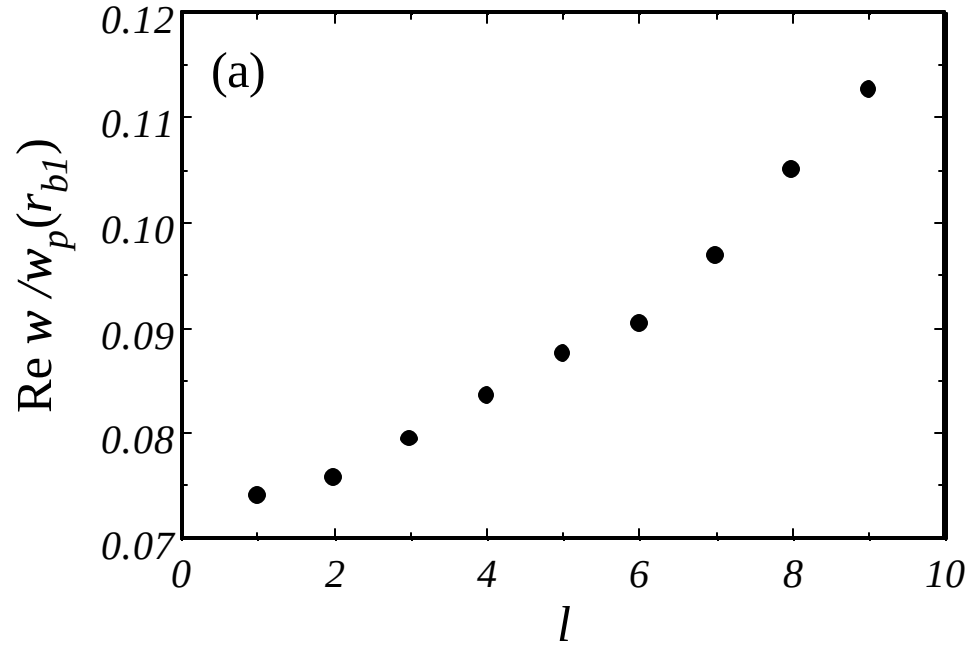
(a)
0.12
0.11
0.10
0.09
0.08
0.07
Re w /w_p(r_b1)
0
2
4
6
8
10
l

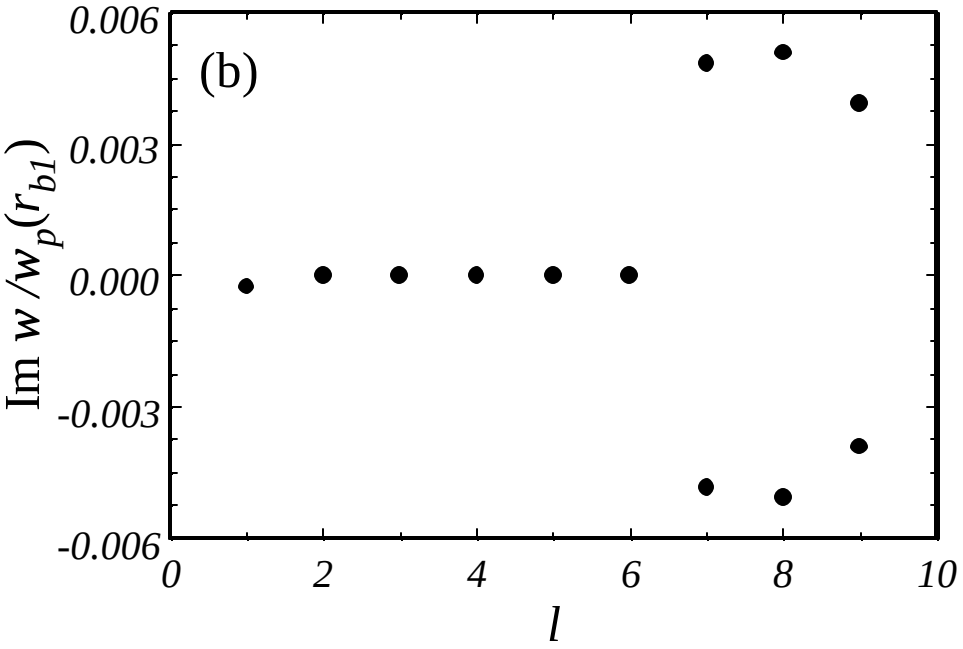
(b)
0.006
0.003
0.000
-0.003
-0.006
Im w /w_p(r_b1)
0
2
4
6
8
10
l

Fig. 4

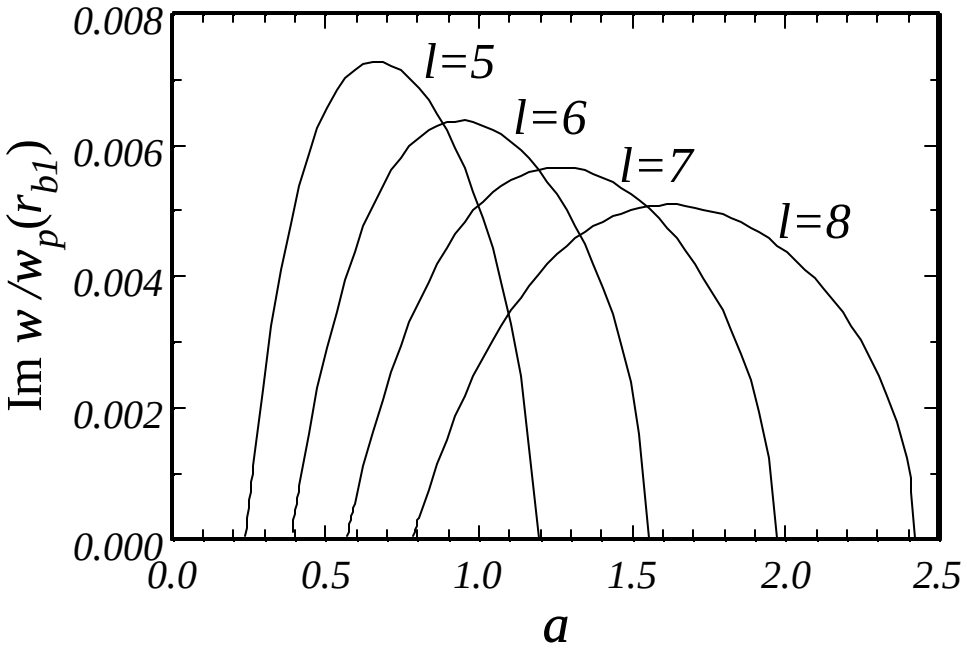

Fig. 5

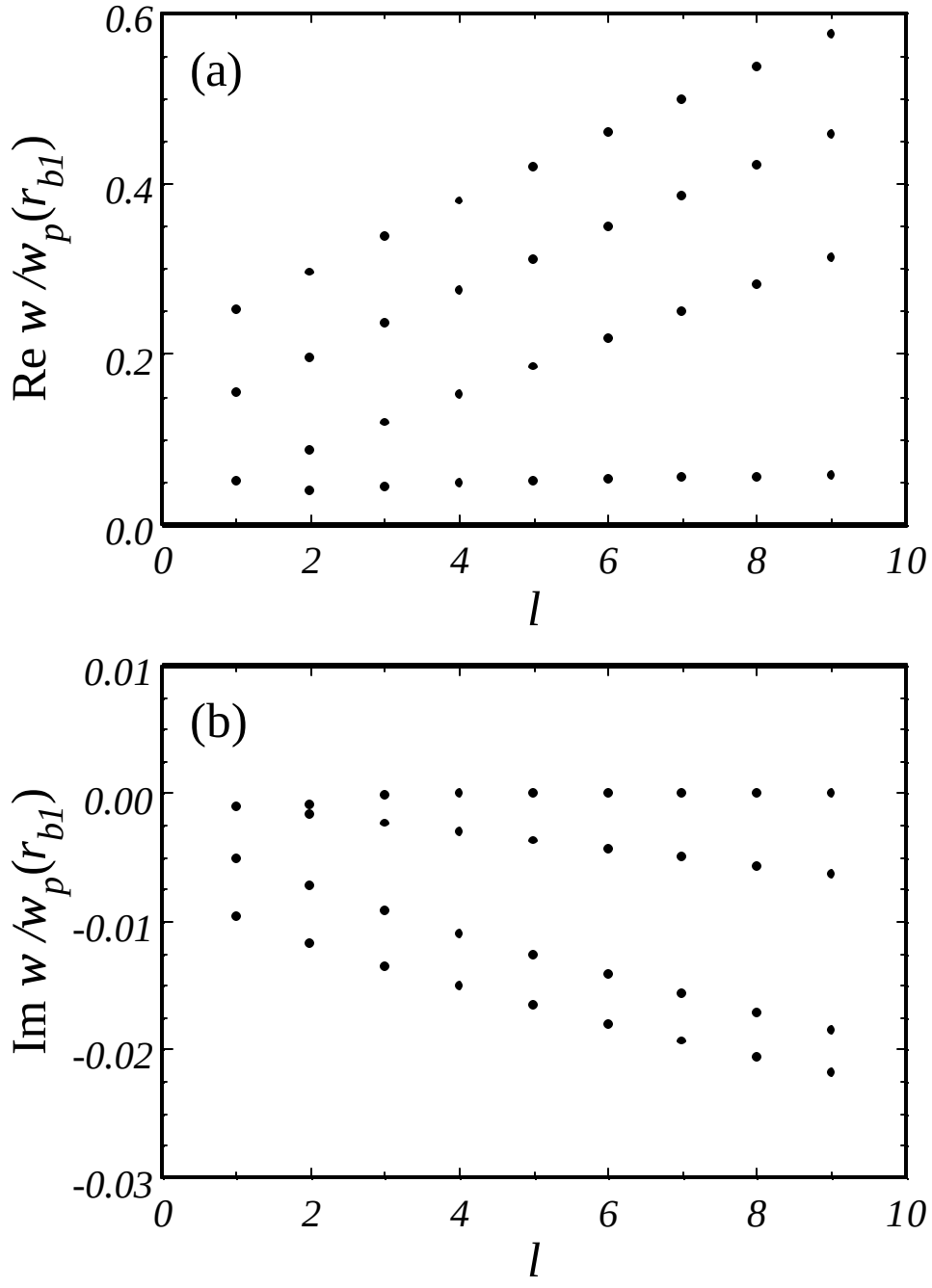
(a)
Re w /w_p(r_b1)
0.6
0.4
0.2
0.0
0
2
4
6
8
10
l
(b)
Im w /w_p(r_b1)
0.01
0.00
-0.01
-0.02
-0.03
0
2
4
6
8
10
l

Fig. 6